# Predicting the occurrence of the vortex ring state for floating offshore wind turbines

Dong, Jing; Viré, Axelle

**DOI**
10.1088/1742-6596/1618/5/052044

**Publication date**
2020

**Document Version**
Final published version

**Published in**
Journal of Physics: Conference Series

Journal of Physics: Conference Series



# Predicting the occurrence of the vortex ring state for floating offshore wind turbines



# Predicting the occurrence of the vortex ring state for floating offshore wind turbines

**Jing Dong, Axelle Viré**

Faculty of Aerospace Engineering, Delft University of Technology, Kluyverweg 1, 2629 HS, Delft, The Netherlands.

E-mail: J.Dong-2@tudelft.nl

**Abstract.** The local aerodynamic loading on floating offshore wind turbines (FOWTs) is more complex than on bottom-fixed wind turbines due to the platform motions. In particular, the FOWT rotor may start to interact with its own wake and enter a so-called vortex ring state (VRS). However, it is still unclear when, and to what extent, the VRS may happen to floating offshore wind turbines. In this paper, we quantitatively predict the VRS using Wolkovitch's criterion during the operating conditions of different FOWTs simulated by FAST. The results show that the type of floating foundation has a significant influence on the aerodynamic performance of the rotor. Also, the probability of occurrence of VRS is bigger for the floating platforms that are more sensitive to wave excitations.

## 1. Introduction

In order to significantly increase the share of wind energy produced worldwide, wind energy technology is moving from onshore to offshore and from shallow water to deep water. Many design challenges however need to be solved to make floating offshore wind turbines (FOWTs) economically attractive. One of them concerns the complex aerodynamics of FOWTs. Due to the combined effects of wind and waves, FOWTs often experience large amplitude motions. It is shown that a FOWT can be subjected to four working states [1] when the floating platform undergoes pitching motion: windmill state, turbulence state, vortex ring state, and propeller state. Generally, when calculating the aerodynamics of bottom-mounted wind turbines, only the windmill working state and the turbulent working state are considered. However, the VRS may seriously influence the aerodynamic performance of FOWTs. Leishman [2] reports the effect of the VRS on a helicopter rotor as follows. First, the rotation becomes apparently unsteady and aperiodic. Second, the blades experience successive forward and backward velocities, which can lead to significant blade flapping and a loss of rotor control. Third, the level of thrust fluctuations is high. Based on this research, we can assume that similar negative effects will occur for FOWTs if not controlled appropriately.

This work aims at predicting how often VRS occurs on FOWTs and to what extent. The NREL 5MW wind turbine is considered for three different floaters (TLP, spar and barge) and subjected to design load cases with regular and irregular waves.

## 2. Methodology to predict the vortex ring state

Even through the momentum theory breaks down when the rotor enters the VRS, it can still be used to predict the occurrence of VRS. Wolkovitch [3] developed a method based on the momentum theory and actuator disk concept to predict the vortex-ring state during the descent of a powered helicopter. The flow model in this theory can be adapted to wind turbines, as illustrated in Figure 1, in which $\mathbf{V}_R$ represents the relative wind velocity related to the actuator disc, $\mathbf{V}_I$ represents the induced velocity at the rotor disc and $\alpha$ represents the angle between $\mathbf{V}_R$ and the rotor disc. The rotor is assumed to be surrounded by a vortex tube. The flow is uniform inside the tube, at any cross section. Outside the tube, the wind speed equals the relative value. This vortex tube is formed of a series of vortex cores. Thus, near the rotor and outside of the tube, the leeward component of stream velocity is $\mathbf{V}_R sin\alpha$, while inside the tube the windward velocity component is $(\mathbf{V}_I - \mathbf{V}_R sin\alpha)$. The velocity of the vortex core center is the average between these velocities, i.e. $(\mathbf{V}_I/2 - \mathbf{V}_R sin\alpha)$ leeward. The vortex ring state is assumed to occur when the relative velocity of the vortex cores normal to the rotor disc falls to zero. Thus the critical velocity $V_{crit}$ associated with Wolkovitch's criterion is given by

$$V_{crit} = \frac{V_I}{2sin\alpha}. \tag{1}$$

This means that when the velocity is lower than the critical velocity, the rotor is in a vortex ring state. Wolkovitch's criterion is considered to predict the VRS when the rotor enters the center of the vortex ring.

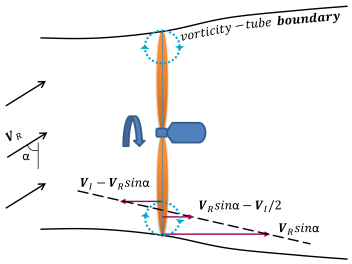


**Figure 1.** Illustration of a stream tube and components of the wind speed in the context of the Wolkovitch's model.

## 3. The wind turbines and platforms

The analysis is performed on the NREL offshore 5MW baseline wind turbine. The basic parameters of the turbine are shown in Table 1. Three types of floaters, namely MIT/NREL TLP, ITI Energy Barge and OC3-Hywind Spar Buoy, have been modified to support the NREL 5MW turbine for realistic simulations. The principal dimensions and hydrostatic data of these platforms are summarized in Table 2. These three types of platforms have different hydrostatic stability characteristics: the stability of MIT/NREL TLP strongly relies on mooring forces; the stability of ITI Energy Barge particularly depends on the restoring force supplied by its freeboard, accordingly it has large waterplane and high CM which make it very sensitive to the surface wave; the stability of OC3-Hywind Spar Buoy mainly comes from the low center of mass (CM) due to the ballast.

**Table 1.** Characteristics of the NREL 5MW reference turbine [4].

| **Rating** | **5MW** |
|---|---|
| Rotor Orientation, Configuration | Upwind, 3 Blades |
| Control | Variable Speed, Collective Pitch |
| Drivetrain | High Speed, Multiple-Stage Gearbox |
| Rotor, Hub Diameter | 126 m, 3 m |
| Hub Height | 90 m |
| Cut-In, Rated, Cut-Out Wind Speed | 3 m/s, 11.4 m/s, 25 m/s |
| Cut-In, Rated Rotor Speed | 6.9 rpm, 12.1 rpm |
| Rated Tip Speed | 80 m/s |
| Overhang, Shaft Tilt, Precone | 5 m, 5°, 2.5° |
| Rotor Mass | 110,000 kg |
| Nacelle Mass | 240,000 kg |
| Tower Mass | 347,460 kg |
| Coordinate Location of Overall CM | (-0.2 m, 0.0 m, 64.0 m) |

## 4. Simulation tool and design load cases

### *4.1. Simulation tool*

The aero-hydro-servo-elastic coupled analysis tool OpenFAST [6] developed by NREL is selected to perform the simulations. OpenFAST enables the calculations with extreme environmental condition, as considered in the present research. We use OpenFAST to output the velocities on the blade sections when the wind turbine is subjected to both wind and waves. These values can be compared to the critical velocities introduced in the previous section, in order to assess whether VRS occurs or not. In this work, the following OpenFAST modules are used: AeroDyn v15 to calculate aerodynamic loads based on blade element momentum (BEM) theory and generalized dynamic wake theory; InflowWind for processing wind-inflow including (but not limited to) uniform hub-height wind and full-field (FF) wind generated from TurbSim; HydroDyn to calculate hydrodynamic loads on a structure with a panel method based on potential-flow theory; MAP++ for mooring loads; ElastoDyn for the structural dynamics; and ServoDyn for control and electrical drive dynamics.

### *4.2. Design load cases (DLCs)*

With irregular waves, we consider the NREL 5MW turbine supported by three different floaters, namely MIT/NREL TLP, ITI Energy Barge and OC3-Hywind Spar Buoy. The IEC design standard prescribes numerous DLCs. Here, in the power production situation, one set of fatigue-type DLCs (NTM+NSS) and one set of ultimate-type DLCs (NTM+ESS) are considered, where NTM stands for normal turbulence wind model, NSS is the normal sea state wave model and ESS is the extreme sea state wave model [5]. The other DLCs described in the design standards with idling or fault of the turbine are not shown here.

According to the requirement of the IEC 61400-3 design standard, the loads analysis shall be based on site-specific external conditions. The present test site is located at 61° 20′ N latitude, 0° 0′ E longitude on the prime meridian northeast of the Shetland Islands, the northeast

**Table 2.** Characteristics of the three floating platforms.

| | MIT/NREL TLP | ITI Energy Barge |
|---|---|---|
| Diameter or width * length | $18m$ | $40m$* $40m$ |
| Draft | $47.89m$ | $4m$ |
| Water displacement | 12,180 $m^3$ | 6,000 $m^3$ |
| Mass, including ballast | 8,600,000 $kg$ | 5,452,000 $kg$ |
| CM location below still water level (SWL) | $40.61m$ | $0.2818m$ |
| Roll inertia about CM | 571,600,000 $kg \cdot m^2$ | 726,900,000 $kg \cdot m^2$ |
| Pitch inertia about CM | 571,600,000 $kg \cdot m^2$ | 726,900,000 $kg \cdot m^2$ |
| Yaw inertia about CM | 361,400,000 $kg \cdot m^2$ | 1,454,000,000 $kg \cdot m^2$ |
| Number of mooring lines | 8 (4 pairs) | 8 |
| Depth to fairleads, anchors | $47.89m$, $200m$ | $4m$, $150m$ |
| Radius to fairleads, anchors | $27m$, $27m$ | $28.28m$, $423.4m$ |
| Unstretched line length | $151.7m$ | 473.3 $m$ |
| Line diameter | 0.127 $m$ | 0.0809 $m$ |
| Line mass density | 116 $kg/m$ | 130.4 $kg/m$ |
| Line extensional stiffness | 1,500,000,000 $N$ | 589,000,000 $N$ |
| | OC3-Hywind Spar Buoy | |
| Width * length | 6.5 to $9.4m$ | |
| Draft | $120m$ | |
| Water displacement | 8,029 $m^3$ | |
| Mass, including ballast | 7,466,000 $kg$ | |
| CM location below still water level (SWL) | $89.92m$ | |
| Roll inertia about CM | 4,229,000,000 $kg \cdot m^2$ | |
| Pitch inertia about CM | 4,229,000,000 $kg \cdot m^2$ | |
| Yaw inertia about CM | 164,200,000 $kg \cdot m^2$ | |
| Number of mooring lines | 3 | |
| Depth to fairleads, anchors | $70m$, $320m$ | |
| Radius to fairleads, anchors | $5.2m$, $853.9m$ | |
| Unstretched line length | $902.2m$ | |
| Line diameter | 0.09 $m$ | |
| Line mass density | 77.71 $kg/m$ | |
| Line extensional stiffness | 384,200,000 $N$ | |

of Scotland[1], as illustrated in Figure 2. The environment data as shown in Table 3 was extracted from the NREL technical report [7] at the same location. We show fifteen NTM+NSS load cases, which are the long-term joint-probability distribution of wind speed $V_\infty$, significant wave height $H_s$, and peak-spectral period of incident waves $T_p$. The NTM+ESS data set is the extreme waves with a 1-year return period ($H_{s1}$, $T_{p1}$) and a 50-year return period ($H_{s50}$, $T_{p50}$), respectively. The fifteen wind speeds of the NTM+NSS data set are also used for the calculations with the extreme wave data (NTM+ESS set). For example, for load case 16 (LC16) $H_{s1}$=10.8m/s, $T_{p1}$=17.6s and $V_\infty$=4.2m/s and for load case 31 (LC31) $H_{s50}$=13.8m/s $T_{p50}$=19.2s

[1] Web site: http://www.waveclimate.com/

**Table 3.** Design load cases

| | | | | | NTM+NSS | | | | | |
|---|---|---|---|---|---|---|---|---|---|---|
| | LC1 | LC2 | LC3 | LC4 | LC5 | LC6 | LC7 | LC8 | LC9 | LC10 |
| $V_\infty$ (m/s) | 4.2 | 5.6 | 7.0 | 8.4 | 9.8 | 11.2 | 12.6 | 14 | 15.4 | 16.8 |
| $H_s$ (m) | 1.7 | 1.8 | 1.9 | 2.0 | 2.2 | 2.4 | 2.7 | 3.0 | 3.4 | 3.7 |
| $T_p$ (s) | 12.7 | 12.7 | 12.8 | 14.8 | 14.1 | 13.4 | 12.7 | 12.1 | 13.4 | 13.4 |
| | LC11 | LC12 | LC13 | LC14 | LC15 | | | | | |
| $V_\infty$ (m/s) | 18.2 | 19.6 | 21.0 | 22.4 | 23.8 | | | | | |
| $H_s$ (m) | 4.1 | 4.5 | 4.8 | 5.2 | 5.5 | | | | | |
| $T_p$ (s) | 15.5 | 14.1 | 13.4 | 16.2 | 15.5 | | | | | |
| | | | | | NTM+ESS 1-YEAR | | | | | |
| $H_{s1}$=10.8m/s $T_{p1}$=17.6s | | | | | | | | | | |
| | | | | | NTM+ESS 50-YEAR | | | | | |
| $H_{s50}$=13.8m/s $T_{p50}$=19.2s | | | | | | | | | | |

and $V_\infty$=4.2m/s.

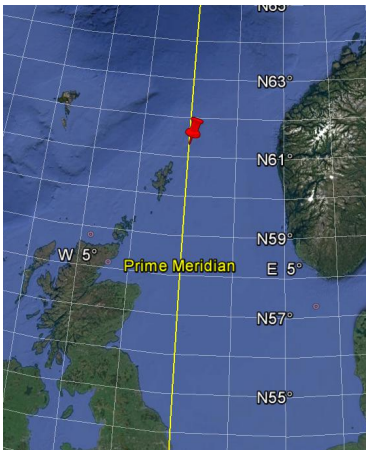


**Figure 2.** Reference-site location.

The default settings in OpenFAST for these simulations are the following. The 6-DOFs platform motions are switched on. The tower and blades are considered as rigid. The free stream wind is defined as full-field 3-component stochastic winds. The blade airfoil aerodynamics model is Beddoes-Leishman (B-L) model and the unsteady airfoil aerodynamic (UA) model is the B-L model developed by Minnema/Pierce. The blade pitch and electrical-drive dynamics control are switched on. The total simulation time is set to 1200s. The initial 300s of each simulation is omitted in the analysis.

## 5. Results and discussion

### *5.1. NREL 5MW turbine mounted on a TLP*

The VRS prediction results of LC1, LC16 and LC31 for the NREL 5MW turbine + MIT/NREL TLP are shown from Figure 3 to Figure 5. The VRS areas predicted with Wolkovitch criterion are shaded in blue, as marked by 'W' in the legends, which represent the occurrence of VRS in a period of time (horizontal axis) and in a particular location on the blade (vertical axis). Additionally, the figures showed the relative wind speed normal to the rotor plane $V_n$ and the 6-DOF platform motions are shown. It can be seen that the VRS areas occur on the outboard part of the blade and coincide with a drop in $V_n$, where the latter is a combined result of the 6-DOF platform motions, the rotor rotation and the wake induction. The occurrence of the VRS in a time span of 1200s has been counted, where we found that in the NSS load case (LC1), some small areas of VRS are found at the outboard part of the blade, with a percentage of occurrence in the time series of 4.66%. In the ESS 1-Year load case (LC16), larger areas of VRS with a percentage of 39.22% along the time span are seen. For the ESS 50-Year load case (LC31), the percentages of VRS is 51.87% according to the Wolkovitch's criterion. The natural period of the surge motion for the TLP is 60.6$s$, which is larger than the wave periods of the load cases considered here (see Table 3) and the natural period of the pitch motion is 4.5$s$, which is smaller than the wave periods. The results show that the low frequency surge motion of the TLP platform is the most sensitive to the wave loads, while the high frequency pitch motion is not sensitive to the wave loads.

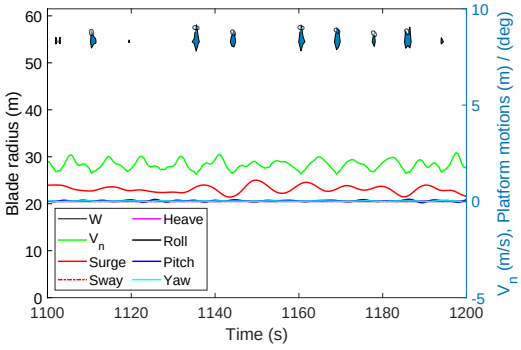


**Figure 3.** TLP with normal irregular waves (LC1)

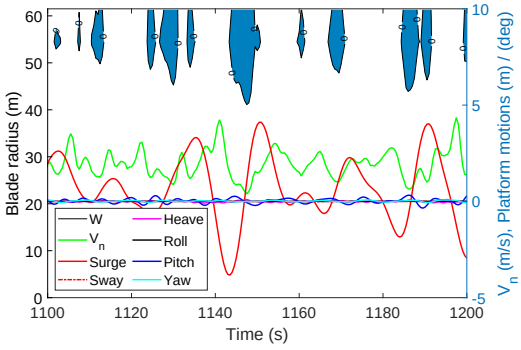


**Figure 4.** TLP with 1-Year extreme irregular waves (LC16)

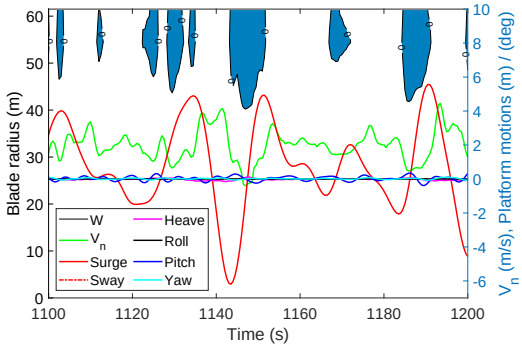


**Figure 5.** TLP with 50-Year extreme irregular waves (LC31)

*5.2. NREL 5MW turbine mounted on the ITI Energy Barge*

The VRS prediction results, $V_n$ and the 6-DOF platform motions of LC1, LC16 and LC31 for the NREL 5MW turbine + ITI Energy Barge are shown from Figure 6 to Figure 8. As for the TLP, the VRS relates to a drop of $V_n$. Most of the VRS areas occur on the outboard part of the blade, but when the value of $V_n$ decreases a lot, the VRS areas extend to the whole blade. For LC1, the percentage of VRS in time series becomes 21.32% based on Wolkovitch's criterion. For LC16 the percentage increases to 49.46% and for LC31 the percentage is 54.87%. The ITI Energy Barge has a natural period in surge of 131.6$s$, which is larger than the wave periods, and a natural period in pitch of 11.8$s$. The results show that the surge and pitch motions of the platform are both sensitive to the wave loads, while the pitch motion has a bigger impact on $V_n$.

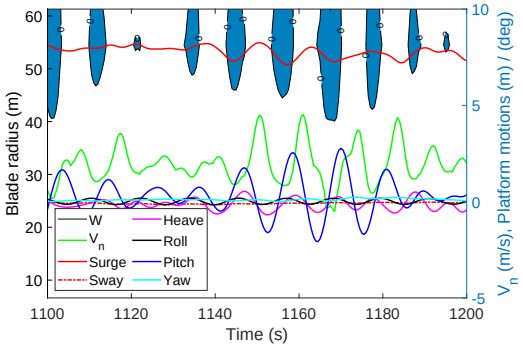


**Figure 6.** Barge with normal irregular waves (LC1)

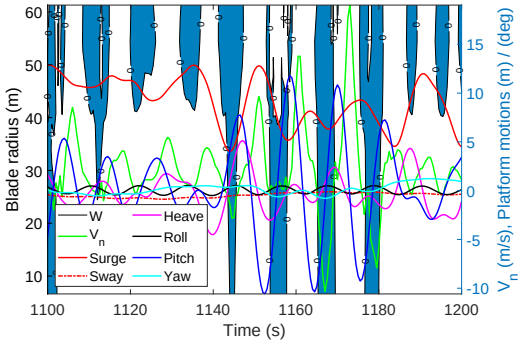


**Figure 7.** Barge with 1-Year extreme irregular waves (LC16)

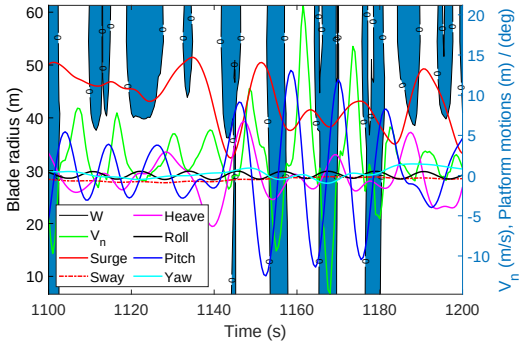


**Figure 8.** Barge with 50-Year extreme irregular waves (LC31)

*5.3. NREL 5MW turbine mounted on the OC3-Hywind Spar*

The VRS prediction results, $V_n$ and the 6-DOF platform motions of LC1, LC16 and LC31 for the NREL 5MW turbine + OC3-Hywind Spar are shown from Figure 9 to Figure 11. Again, the VRS occurs with the drop of $V_n$. Most of the VRS areas occur on the outboard part of the blade. As for the barge, the VRS areas extend to the whole blade when the value of $V_n$ decreases sharply. As for the TLP, the percentages of VRS of LC1, LC16 and LC31 are 16.82%, 43.96% and 51.37%, respectively. The natural periods of the surge and pitch motions for the

OC3-Hywind spar are 125.0$s$ and 29.2$s$, respectively, which are both larger than the wave periods of these load cases. The results show that the surge and pitch motions of the OC3-Hywind Spar platform are both sensitive to the wave loads.

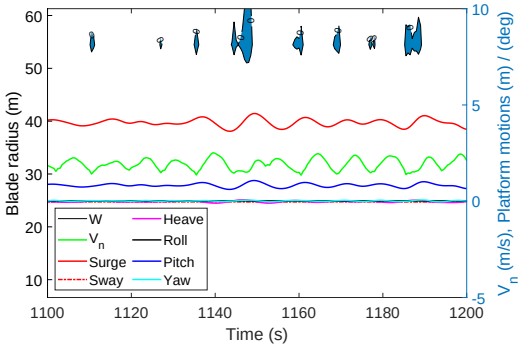


**Figure 9.** Spar with normal irregular waves (LC1)

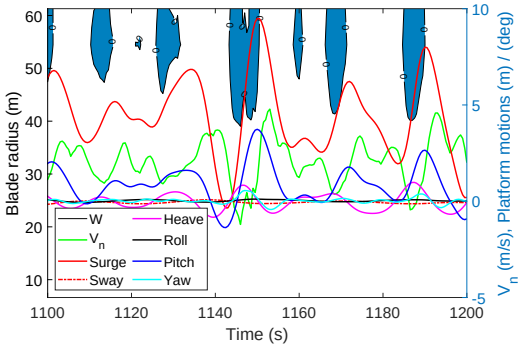


**Figure 10.** Spar with 1-Year extreme irregular waves (LC16)

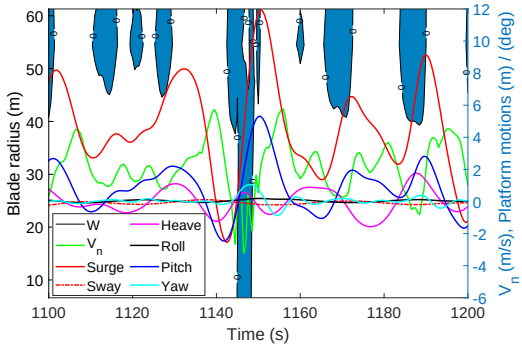


**Figure 11.** Spar with 50-Year extreme irregular waves (LC31)

*5.4. Summary of the VRS performance of these three types of platforms*

Figure 12, Figure 13 and Figure 14 show the percentage of VRS for all the NSS and ESS load cases as listed in Table 3 for the MIT/NREL TLP, ITI Energy Barge and OC3-Hywind Spar respectively. The results show that the VRS is more likely to happen in a low wind speed region. For all the three types of platforms, the VRS wind speeds extend to 8.4m/s, 15.4m/s and 12.6m/s respectively. For the ESS 50 Year and ESS 1 Year load cases, all the three types of platforms have a significant VRS occurrence. For the NSS load cases, the TLP shows better sea keeping ability than the two other platforms and has the least chance of VRS occurrence. By contrast, the ITI Energy Barge is the most sensitive to the wave load and the largest probability of occurrence of VRS. It is worth noting that the maximum percentages of the VRS for different types of platform are roughly the same, which are all around 50%. This is because the rotor motion of FOWTs is periodic and the VRS only occurs during the leeward motion of the rotor. When the rotor moves backward, $V_n$ increases and the VRS disappears.

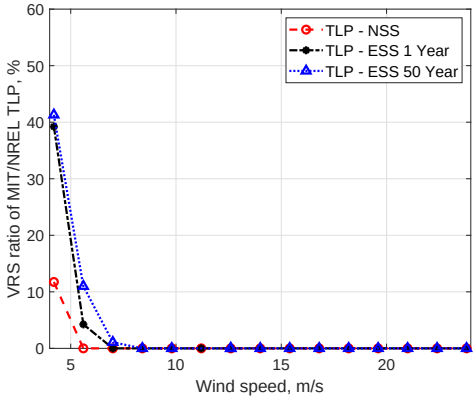


**Figure 12.** The VRS ratio of MIT/NREL TLP.

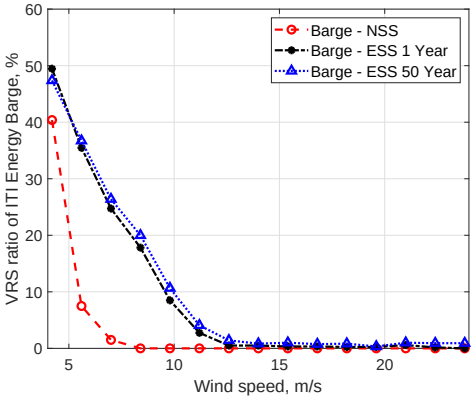


**Figure 13.** The VRS ratio of ITI Energy Barge.

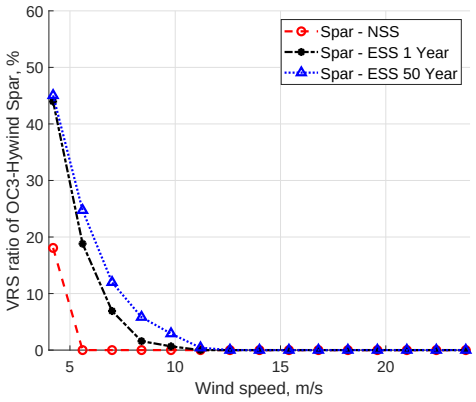


**Figure 14.** The VRS ratio of OC3-Hywind Spar.

*5.5. Thrust characteristics in the VRS region*

Taking the ITI Energy Barge as an example, we analyzed the characteristics of the thrust force in the VRS region. Figure 15, Figure 16 and Figure 17 show the standard deviations and the mean values of the thrust force along the blade for LC1, LC16, and LC31, respectively. In these figures, the results of nine nodes spaced equally along the blade are evaluated. From the above analysis, it can be seen that the maximum rate of VRS occurs at around node 8, which corresponds to a radius of $r = 54.458m$. The present results show that both the standard deviation and the mean value of the thrust force are maximum at node 8, which means that the thrust force in the VRS region is relatively big and has strong variation. This observation is in line with that of Leishman [2], which showed that helicopter rotors are difficult to control and have high levels of thrust fluctuations during the onset of VRS.

## 6. Conclusions

The vortex ring state is a critical working state that can significantly affect the performance and lifetime of FOWTs. In this work, the probability of occurence of VRS is computed for different floaters and load cases. The results show that the type of floating foundation has a significant influence on the aerodynamic performance of the rotor. As expected, the TLP exhibits the least motions, and therefore, also the least probability of occurrence of the VRS. Also, the probability

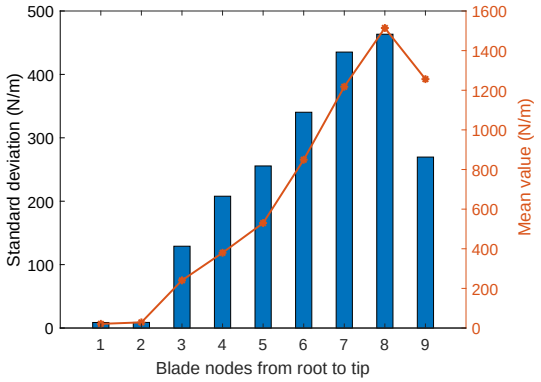


**Figure 15.** Standard deviation and mean thrust - LC1.

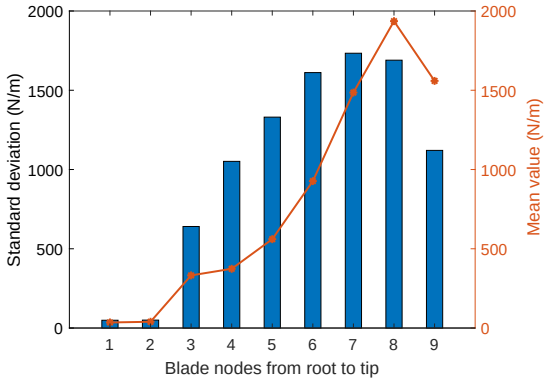


**Figure 16.** Standard deviation and mean thrust - LC16.

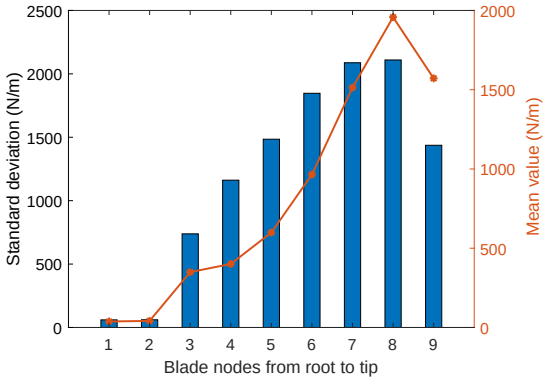


**Figure 17.** Standard deviation and mean thrust - LC31.

of occurrence of VRS generally increases with the magnitude of the wave height, except in cases where the velocity normal to the rotor exhibits large fluctuations. However, importantly, for all the platform types, the turbine presents a risk of experiencing the vortex ring state even under normal sea states. This work provides insight in how FOWTs can be better designed and controlled to mitigate the risk of VRS.

### *6.1. Acknowledgments*

Dong would like to acknowledge the support from China Scholarship Council (CSC).

## References

[1] Sebastian T, Lackner M A 2013 *Wind Energy* Characterization of the unsteady aerodynamics of offshore floating wind turbines. **16(3)** 339–352
[2] Leishman J G 2006 *Principles of Helicopter Aerodynamics* Cambridge University Press, Cambridge.
[3] Wolkovitch J 1972 *J. Am. Helicopter Soc* Analytical prediction of vortex-ring boundaries for helicopter in steep descents. **17** 13–19
[4] Jonkman J and Butterfield S and Musial W and Scott G 2009 *NREL* Definition of a 5-mw reference wind turbine for offshore system development.
[5] Jonkman J and Sprague M 2018 *NWTC Information Portal (OpenFAST)* https://nwtc.nrel.gov/OpenFAST.
[6] IEC 61400–3 2009 *IEC* Wind Turbines – Part 3: Design Requirements for Offshore Wind Turbines.
[7] Jonkman J M 2007 *NREL* Dynamics modeling and loads analysis of an offshore floating wind turbine. Technical Report NREL/TP-500-41958